ELECTRONIC SUPPLEMENTARY INFORMATION

Organo-Disulfide-Based Particles Enable Controlled Stimulus-Triggered Cleaning of Electrode Surfaces

Hongyi Zhang,[a,b] Garrett L. Grocke,[a,b] Samuel S. Kopfinger,[a] Yilin Wang, [b, e, f] Arnav Brahmasandra,[a] Randy H. Ewoldt,[b, e, f] Stuart J. Rowan[a,b,c,d*] and Shrayesh N. Patel[a,b,c*]

a. Pritzker School of Molecular Engineering, University of Chicago, Chicago, Illinois 60637, USA

b. Joint Center for Energy Storage Research, Argonne National Laboratory, Argonne, IL 60439, USA

c. Chemical Sciences and Engineering Division, Argonne National Laboratory, Argonne, IL 60439, USA

d. Department of Chemistry, University of Chicago, Chicago, Illinois 60637, USA
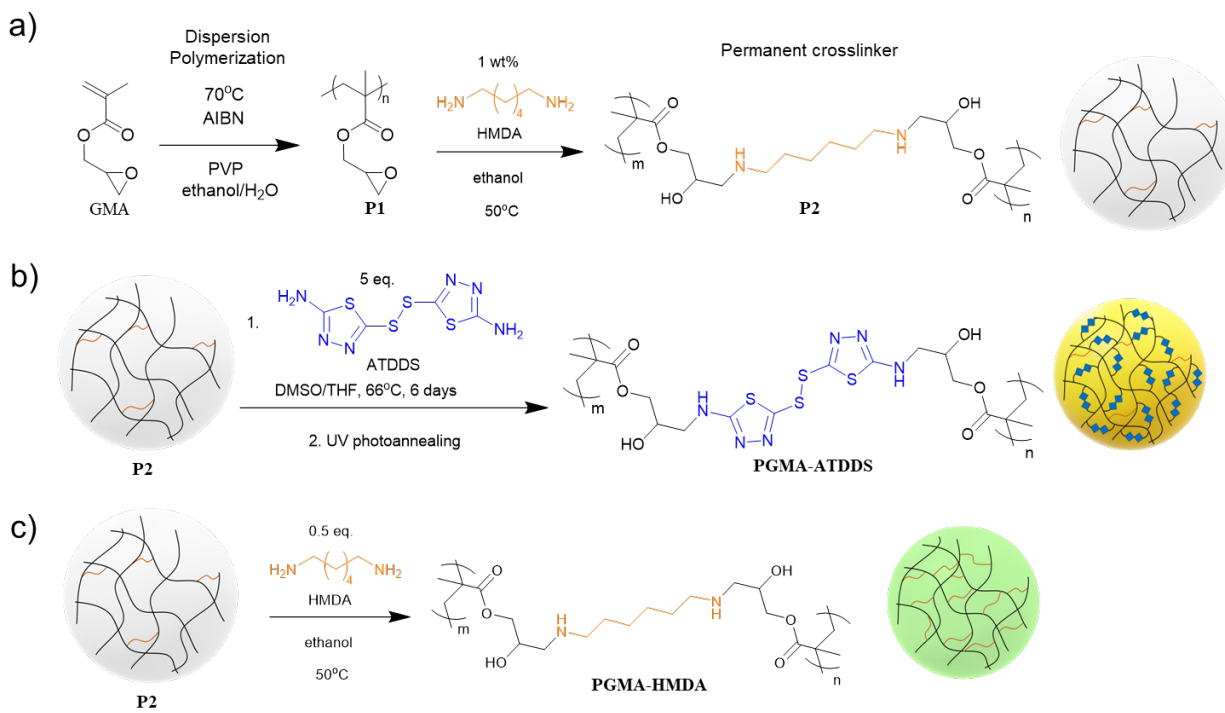
e. Department of Mechanical Science and Engineering, University of Illinois Urbana-Champaign, Urbana, Illinois 61801, USA

f. Beckman Institute for Advanced Science and Technology, University of Illinois Urbana-Champaign, Urbana, Illinois 61801, USA

*corresponding authors: stuartrowan@uchicago.edu, shrayesh@uchicago.edu

Contents:

Scheme S1. a) Synthesis of P1 and P2 particles. b) Synthesis of PGMA-ATDDS particles from P2 particles. c) Synthesis of PGMA-HMDA particles from P2 particles.
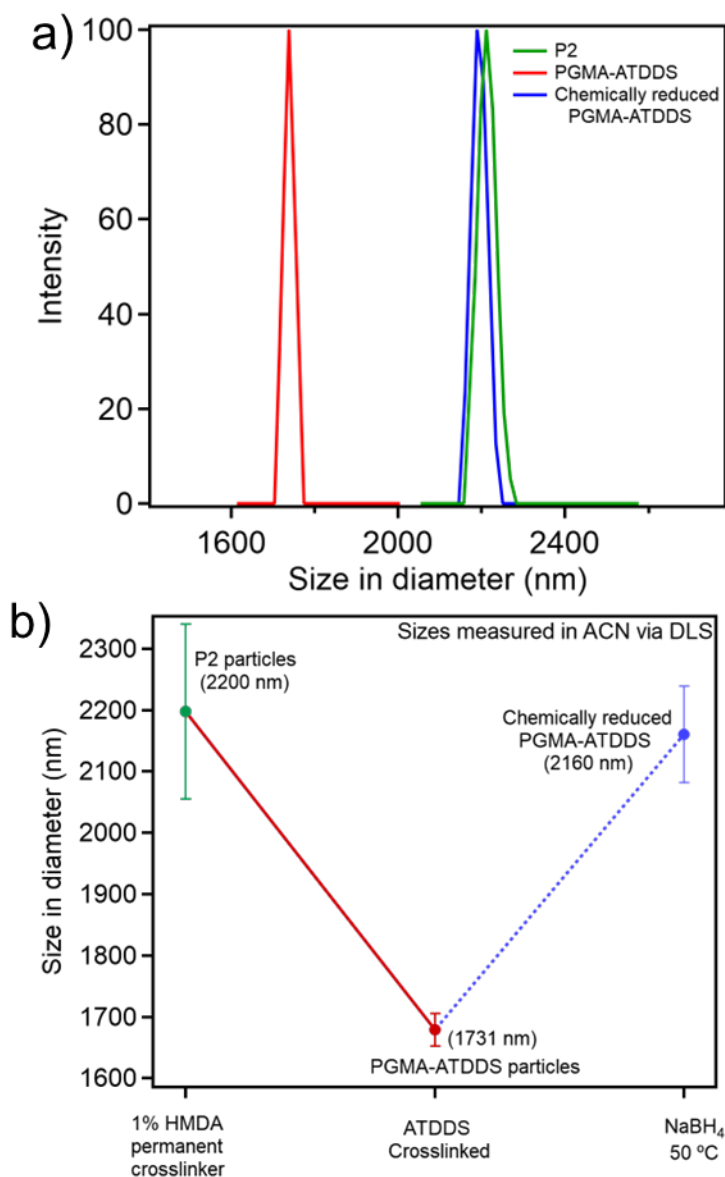
Figure S1. a) Representative size measurement using dynamic light scattering (DLS) of the P2 particles, PGMA-ATDDS particles, and chemically reduced PGMA-ATDDS particles in a 0.1 mg/mL suspension in acetonitrile (ACN). b) Averaged particle size across three DLS measurements of the P2 particles, PGMA-ATDDS particles, and chemically reduced PGMA-ATDDS particles
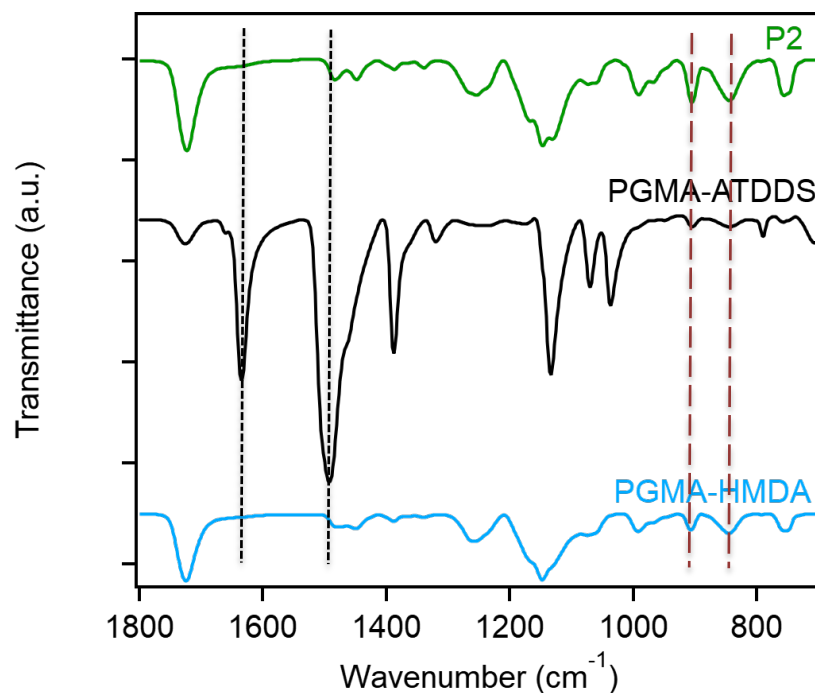
Figure S2. FT-IR spectra of lightly crosslinked PGMA (P2), PGMA-ATDDS and PGMA-HMDA.

Shimadzu IRTracer-100 FT-IR with single bounce attenuated total reflection ATR diamond was used to characterize all polymer particles. The sample powder (~ 10 mg) was placed directly onto the ATR crystal. Carbonyl peak at 1722 cm^{-1} was observed for particles at all functionalization states. Characteristic epoxy peaks at 846 cm^{-1} and 905 cm^{-1} indicate the symmetric and asymmetric stretching of the bonds (highlighted with right two dotted lines red lines). The decrease in epoxy peaks in PGMA-ATDDS and emerged peaks centered at 1668 cm^{-1} and 1508 cm^{-1} (highlighted with left two dotted black lines) attributed to N-H bending confirm the amination of epoxide groups. PGMA-HMDA showed no addition peak with decrease in epoxy peaks at 846 cm^{-1} and 905 cm^{-1} indicating successful reaction of P2 with additional HMDA.
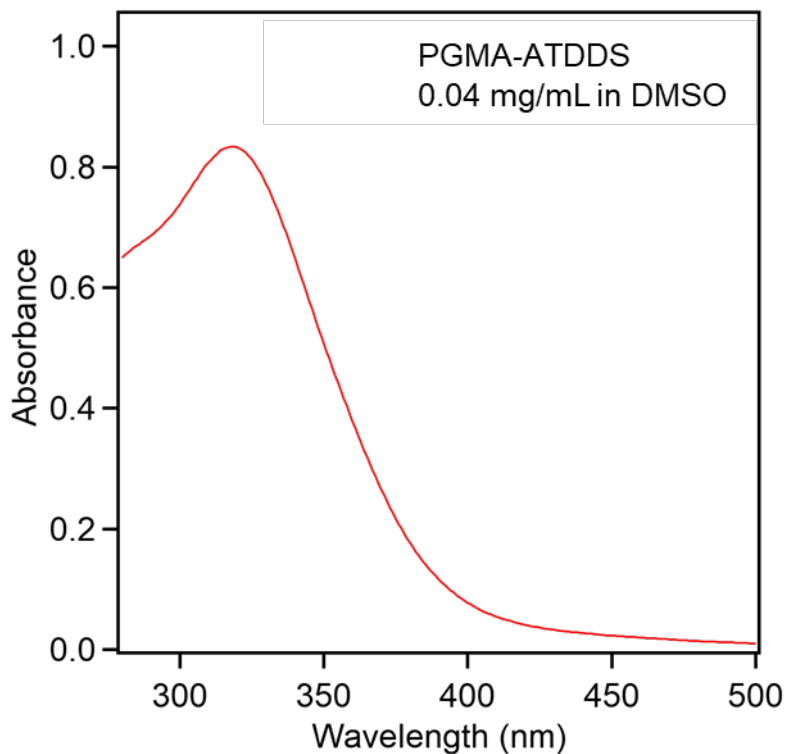
Figure S3. UV-Vis absorbance spectra for covalently-bound ATDDS on PGMA-ATDDS dispersion in DMSO.

A Shimadzu UV-3600 Plus UV-Vis-NIR spectrophotometer was employed for measuring absorbance in the wavelength range spanning from 250 nm to 500 nm, utilizing a sampling interval of 1 nm. A suspension of PGMA-ATDDS at a concentration of 0.04 mg/mL in DMSO was used for characterization.
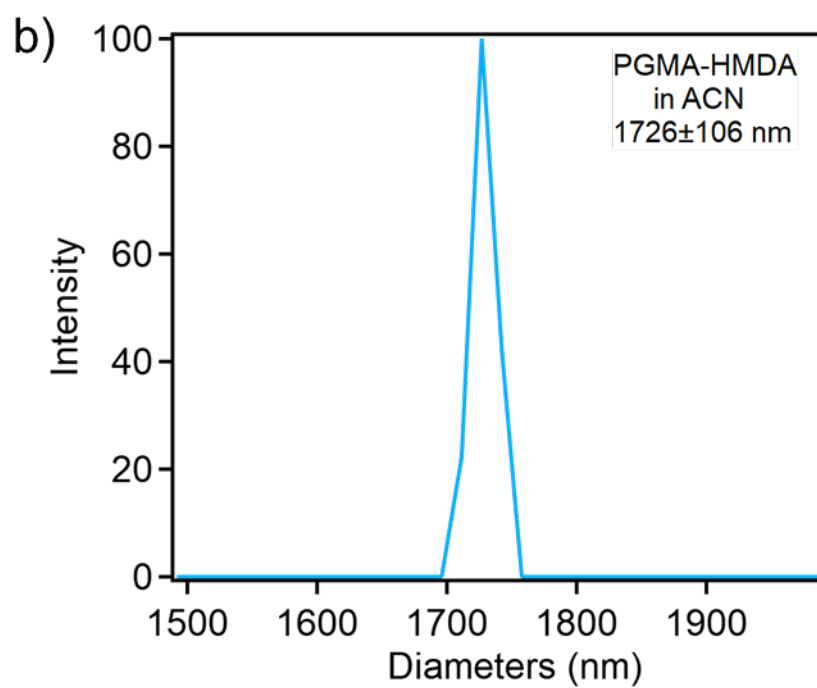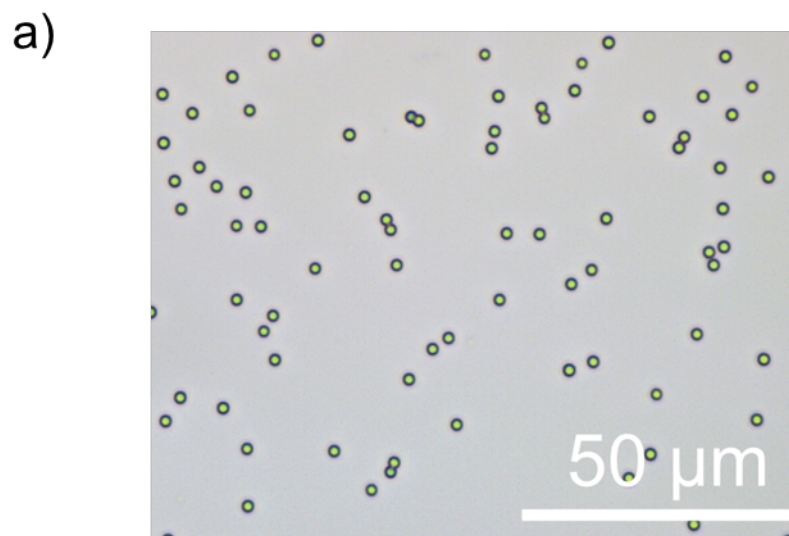
Figure S4. a) Optical image and b) DLS of PGMA-HMDA in ACN
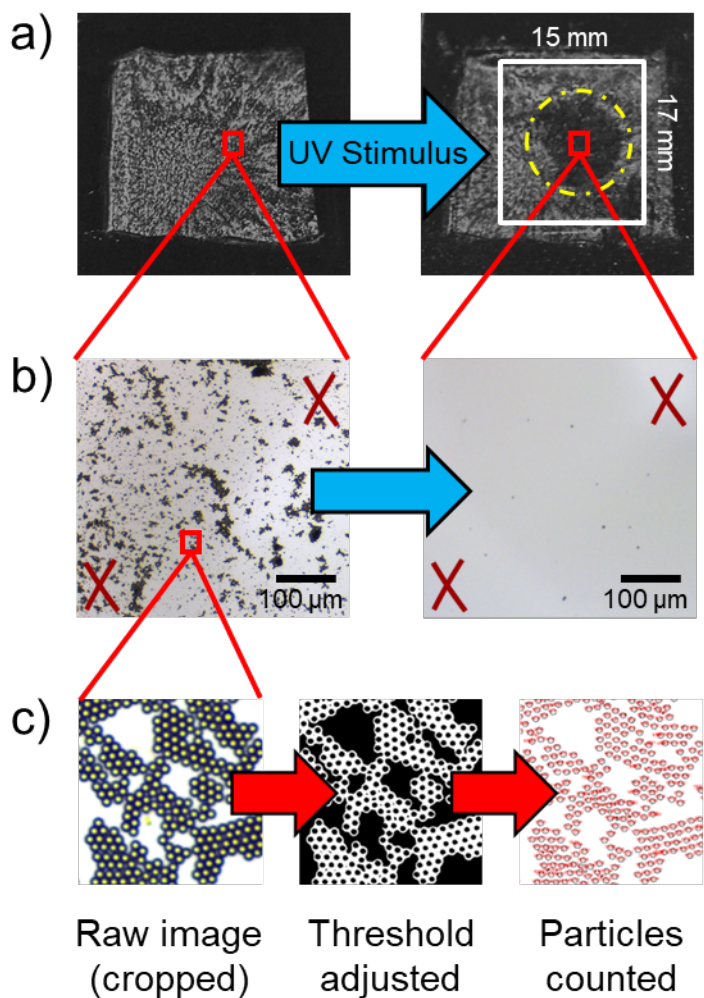
Figure S5. a) Direct observation shows 2D substrates before and after particle removal. Yellow dashed circle indicates area exposed to UV stimulus via fiber optic source. b) Markers (red X) are used to find the same spots before and after testing (Note – the markers are etched onto the back of the substrate, and therefore can't be simultaneously imaged with the particles). c) Image analysis of 50 times magnification images resulting in particle counting.

a)

Backing plate (5.72 x 5.72 x 0.58 cm) and ITO substrate (1.1 mm thick with 100 μm of ITO)

PTFE gasket (50 μm thick)

Positive electrode (3 mm thick) with flow channels

Flow cell body (5.72 x 5.72 x 1.95 cm) with connectors

b)

Electrochemical electrode cleaning setup

UV light source

UV electrode cleaning setup

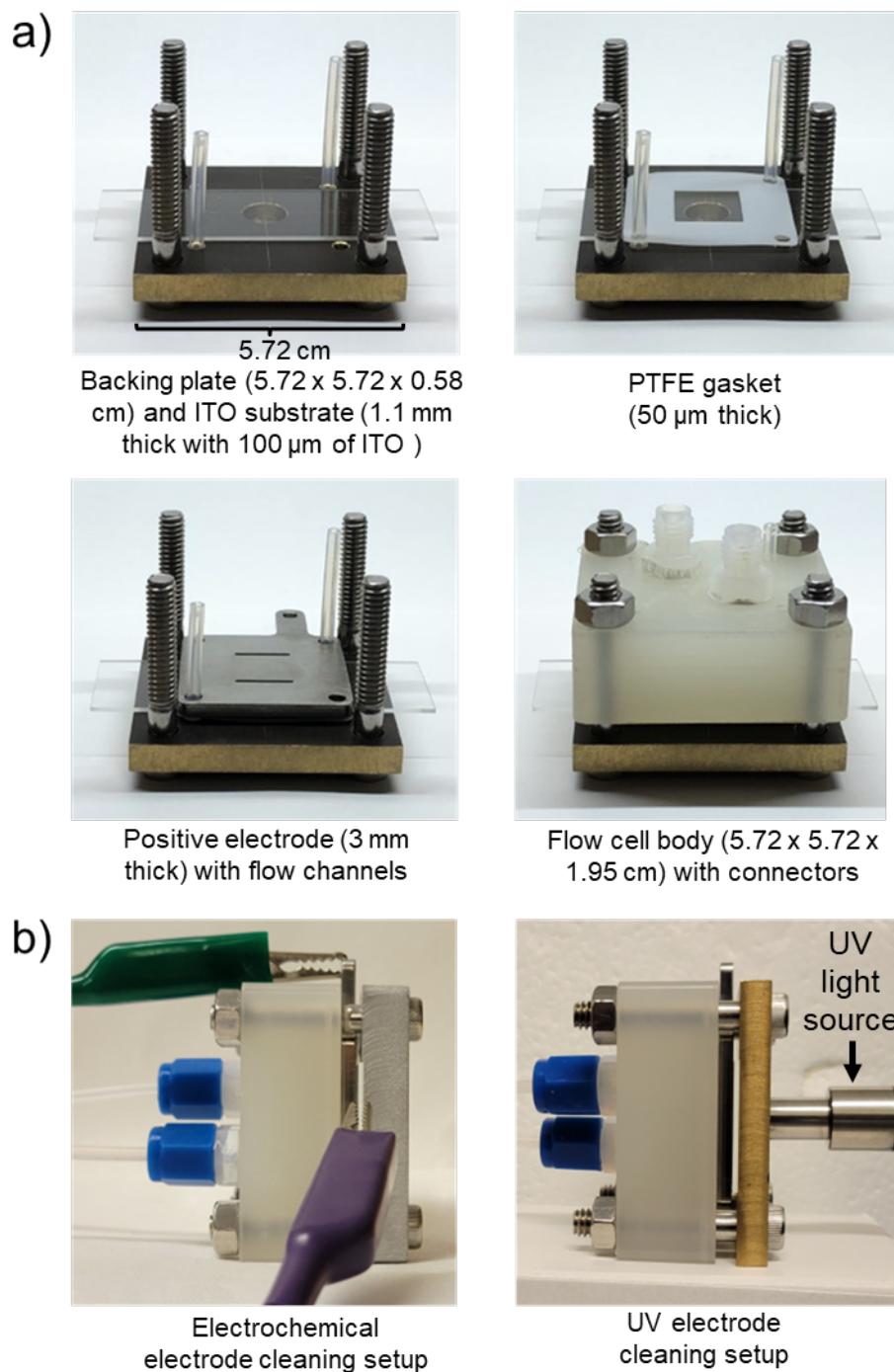**Figure S6.** Design of modular half flow cell electrode cleaning apparatus. a) Assembly of flow cell with backing plate, ITO substrate, PTFE gasket, positive electrode with flow channels and flow cell body with connectors. b) Installation of stimuli source: electrical leads for electrochemical electrode cleaning setup, or UV fiber optic for UV electrode cleaning.
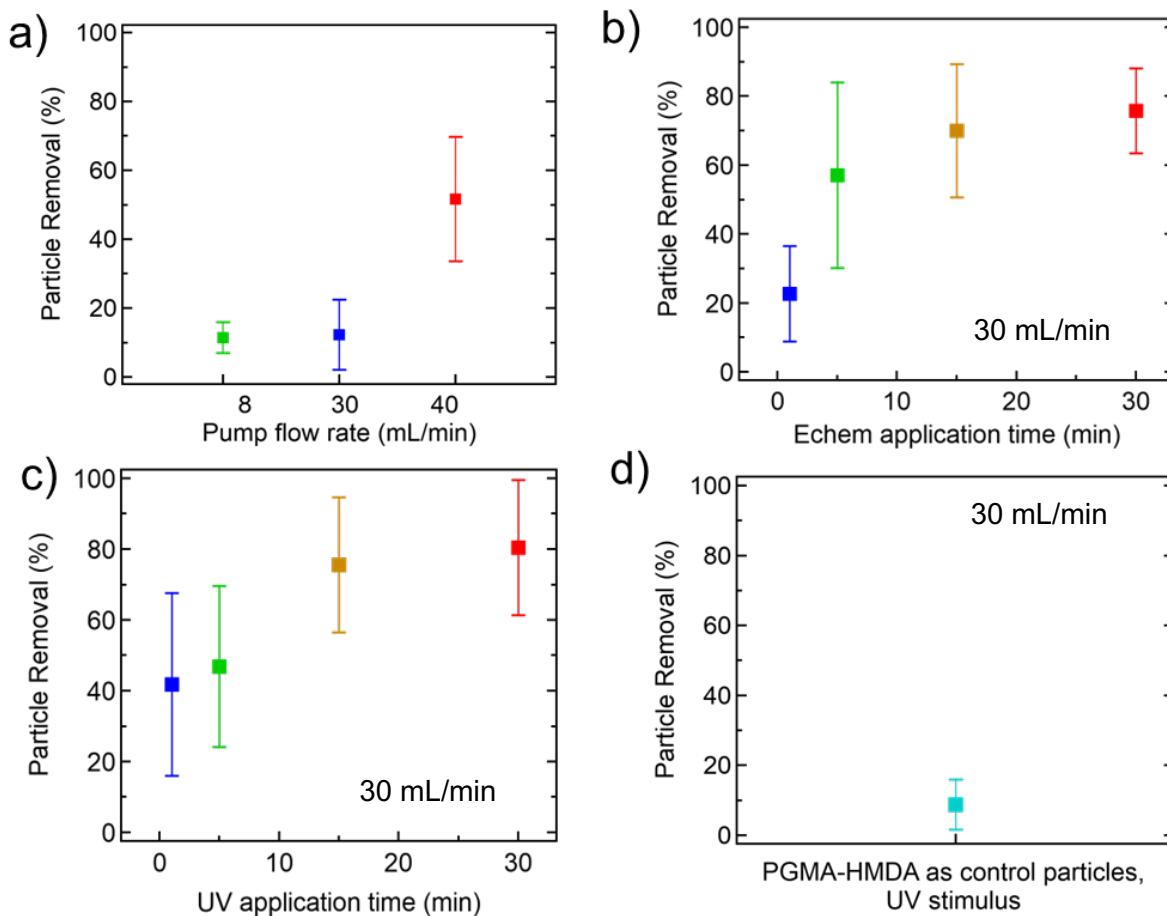
Figure S7. Particle removal from 2D substrates via controlled stimulus under shear flow conditions. a) Experimental flow rate determination with no stimulus, 30 min of flowing with a liquid electrolyte (100 mM $TBAPF_6$ in ACN). b) Time-dependent particle removal with electrochemical stimulus (under constant potential of 2 V, approximately -1.7 V vs Ag/Ag$^+$, applied across the whole cell) c) UV photoexcitation stimulus (irradiated via a light source with intensity of 1 W/cm^2 was secured into the optical viewport on the backside of the stainless steel plate supporting the artificially-fouled substrate) and d) PGMA-HMDA as control particles under UV stimulus at 30 mL/min of flowing with a liquid electrolyte (100 mM $TBAPF_6$ in ACN).

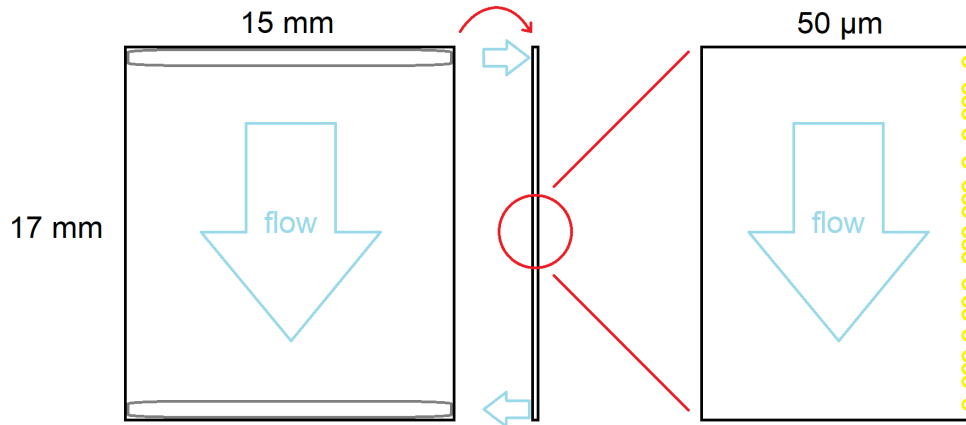**Figure S8.** Geometry of the flow channel of the electrode cleaning flow cell. The small gap (50 μm) is set by the thickness of the PTFE gasket. Left: planar view of the flow field. Right: cross section view of the flow field.

The small gap of the flow channel creates a laminar slit flow and enables analytical calculation of the wall shear stress, which we describe here. For Newtonian fluids flowing in a rectangular slit at a constant flow rate, Q, the shear rate at the wall, $\dot{\gamma}_w$, is related to the flow rate as,

$$\dot{\gamma}_w = \frac{6Q}{wh^2},$$

where w and h are the width and the depth of the slit respectively.[1]

For Newtonian fluids, the shear stress at the wall, τ_w, can be calculated by $\tau_w = \dot{\gamma}_w \cdot \mu$, where μ is the Newtonian viscosity of the fluid. The viscosity of fluid is $\mu = 0.507$ mPa.s, as measured with a rotational rheometer using a double gap rotor and cup cylinder (TA Instruments ARES-G2). Additional experimental validation was performed with a microfluidic slit-flow viscometer (m-VROC, Rheosense) with a similar small gap and direct pressure measurement to verify laminar flow (via Reynolds number), and calculate shear viscosity, shear rate, and wall shear stress.

The Reynolds number, Re, is calculated to check for the laminar flow assumption, where

$$Re = \frac{\rho U h}{\mu}.$$

When Re is lower than the critical transition number of 2300, flow is laminar and the shear rate and stress can be calculated by the methodology above.[2] In both the actual cell and the microfluidic viscometer, Re is calculated, shown in Table S1. We find that Re ranges from 18 – 88 across all conditions, verifying laminar flow.

With laminar flow established, the wall shear rate and wall shear stress can be computed from the aforementioned equations, with results shown in Table S1. The wall shear rate is high, ranging from about 21,000 to 110,000 s^{-1}. With the low viscosity electrolyte, this gives a wall shear

stress ranging from 10 – 54 Pa, a range that is consistent with the yield stress of soft viscoplastic solids.[3]

In the microfluidic viscometer, four pressure sensors are mounted at the boundary wall along the flow channel, the shear stress therefore can be directly computed by monitoring the pressure drop as

$$\tau_w = \frac{\Delta P}{L} \frac{wh}{2w + 2h}$$

where ΔP is the measured pressure drop, and L is the channel length over which ΔP is measured (15 mm).

From the wall shear stress, the resulting force on a single particle can be estimated by

$$f = \tau_w A = \tau_w \frac{\pi D^2}{4}$$

where D is the diameter of the particle (~1731 nm). A range from 25 to 130 pN is estimated, as shown in the last column of **Table S1**.

Table S1. Flow calculations for narrow channel flow field.

w	h	Q	$\dot{\gamma}_w$	Velocity (U)	τ_w	Re [4]	f
[mm]	[μm]	[mL/min]	[s^{-1}]	[m/s]	[Pa]	[-]	N (x10^{-11})
Calculations based on actual cell geometry							
15	50	8	21,000	0.178	**10**	18	2.5
15	50	30	80,000	0.667	**41**	66	9.5
15	50	40	110,000	0.889	**54**	88	13
Experimental validated values via microfluidic viscometer							
2*	51.3*	1.8*	34,200*	0.292*	17.3*	29.6*	4.1

*The dimensions and flow rate here are the dimensions of microfluidic viscometer and the maximum flow rate it can achieve.[4]

Experimental data obtained through microfluidic viscometry have confirmed the validity of the calculations for the custom flow cell's geometry, shown in the final row of Table S1. These results provide strong evidence that the particles within the flow cell are indeed experiencing laminar flow.
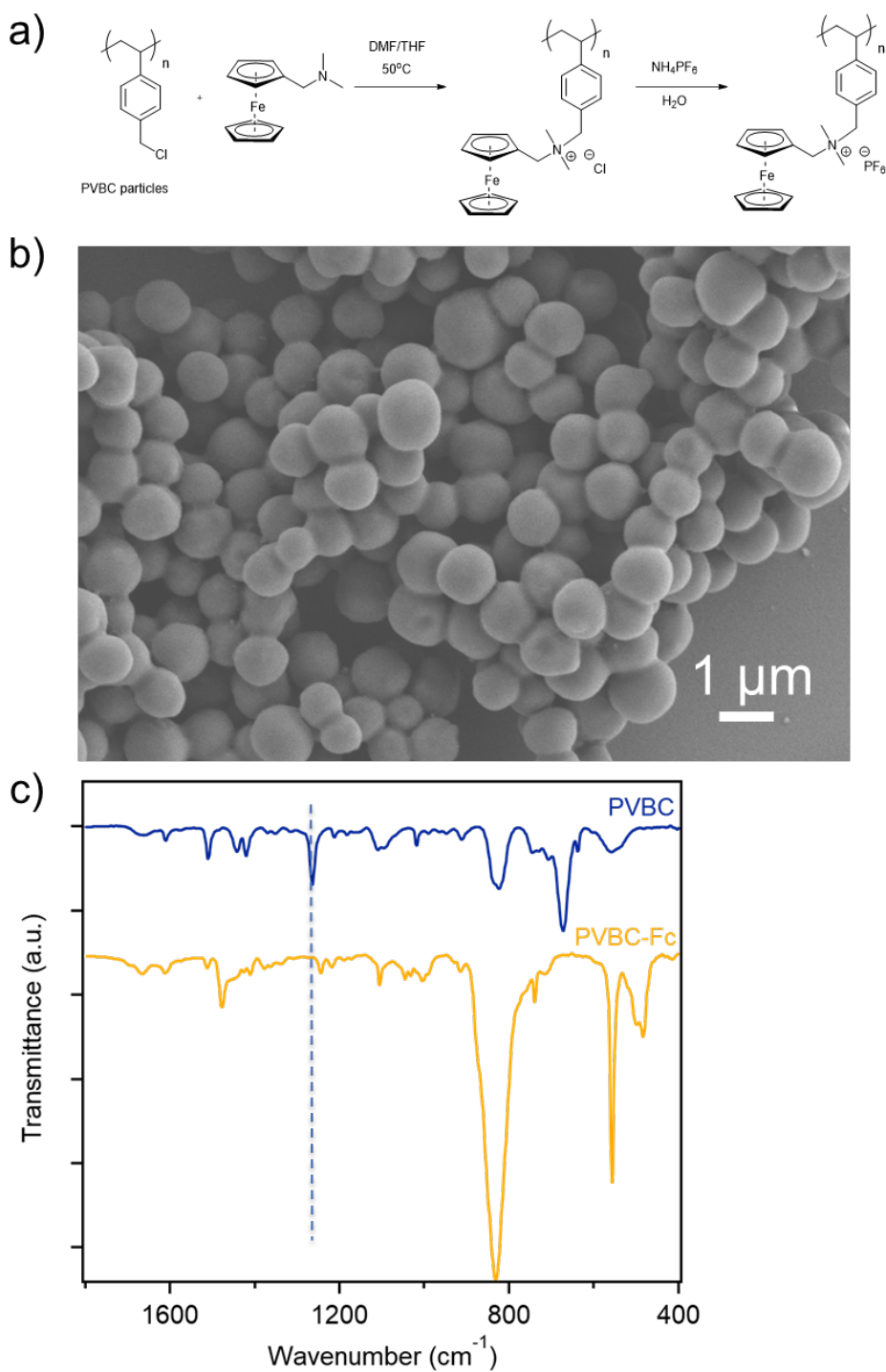
Figure S9. a) Synthetic scheme for PVBC-Fc particles for electrode regeneration experiment. b) SEM image of PVBC-Fc particles. c) FT-IR spectra of PVBC particles and PVBC-Fc particles. The disappearance of 1265 cm^{-1} (highlighted with the dotted blue line), which assigned to -CH$_2$Cl wagging vibration in PVBC indicating the successful functionalization of PVBC with (dimethylamino)ferrocene to yield PVBC-Fc.[5]
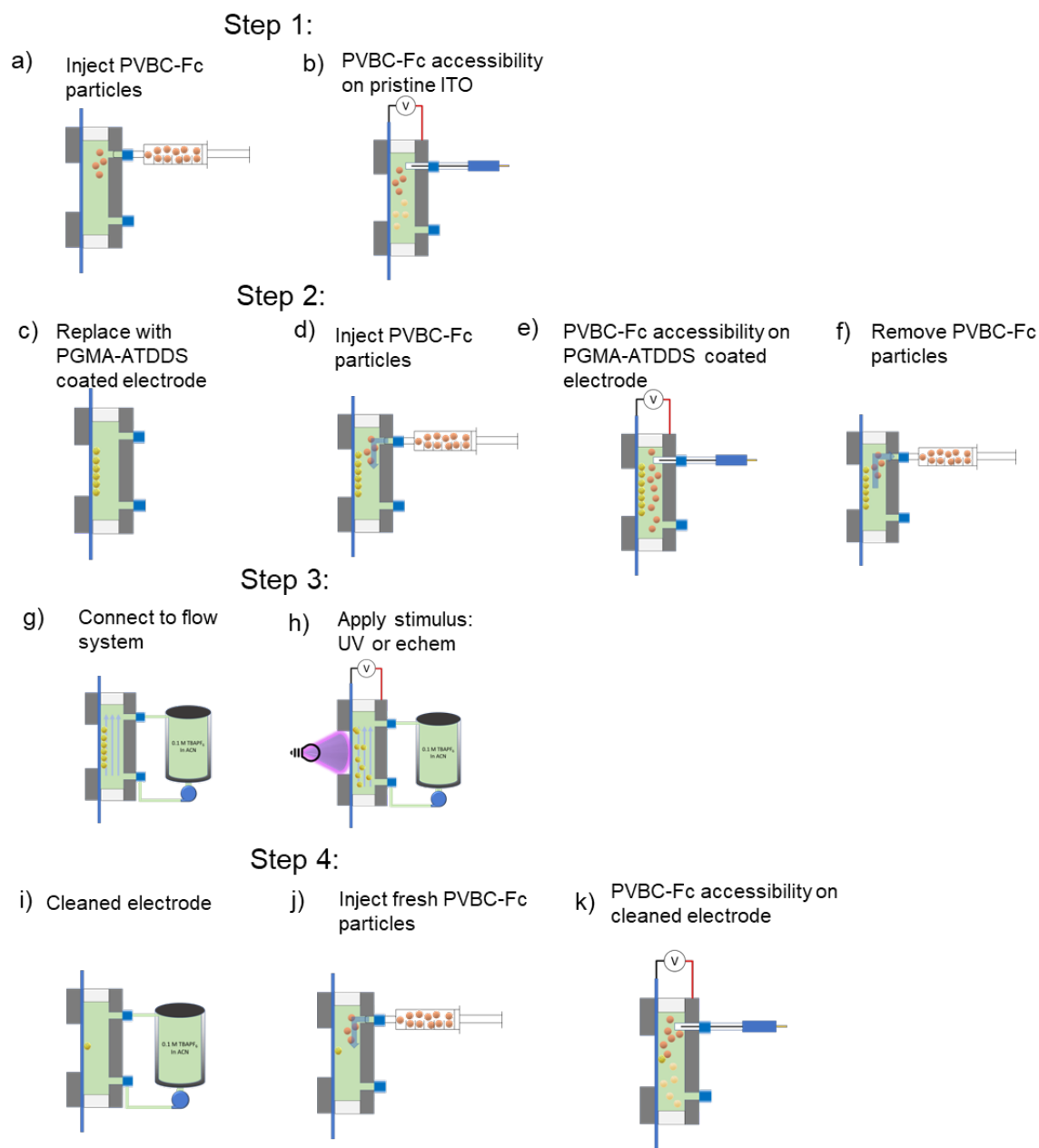
Figure S10. Step 1: a) Inject PVBC-Fc particles dispersion into the custom static flow cell with pristine ITO electrode. b) Measure electrochemical response of PVBC-Fc on pristine ITO electrode. Step 2: c) Manually clean ITO electrode to remove remaining PVBC-Fc and artificially fouled with PGMA-ATDDS d) Inject fresh PVBC-Fc dispersion. e) Measure the electrochemical response of PVBC-Fc on PGMA-ATDDS coated ITO electrode. f) Remove PVBC-Fc. Step 3: g) Connect flow cell with coated electrode to pump. h) Cleaning procedure is performed with either electrochemical or UV photoexcitation stimulus. Step 4: i) Remove stimulus to yield cleaned electrode. j) Disconnect the flow cell with pump and inject PVBC-Fc. k) Measure the electrochemical response of PVBC-Fc on cleaned electrode.
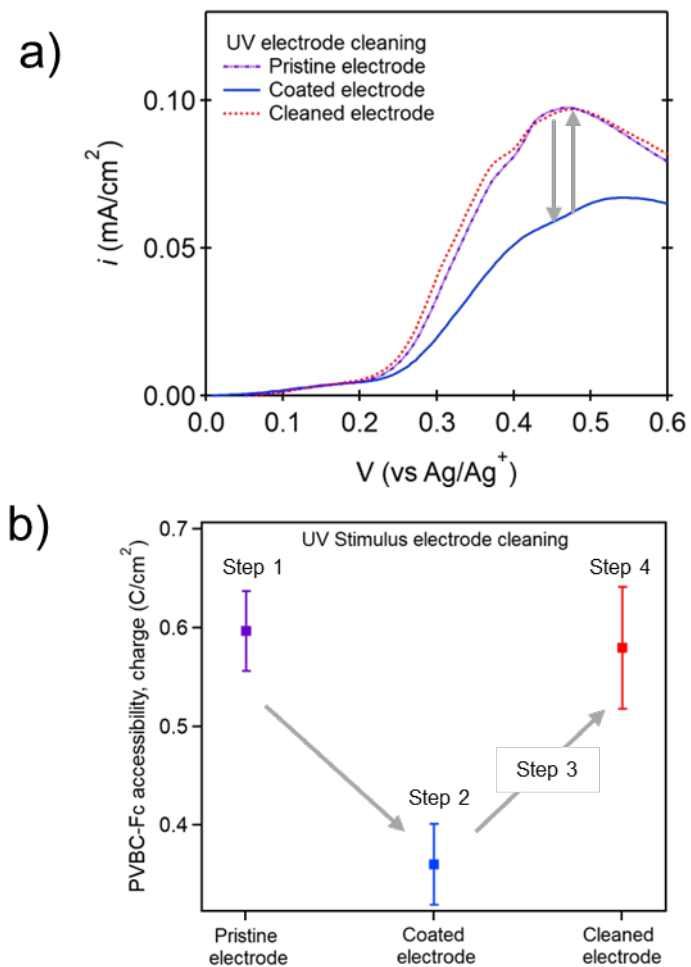
Figure S11. a) Linear sweep voltammetry (LSV) curves for PVBC-Fc activity at ITO electrode surface, showing performance of a clean electrode and a fouled electrode before and after UV electrode cleaning. b) PVBC-Fc accessibility in terms of charges for UV stimulus electrode cleaning.

References

1   C. W. Macosko, *Rheology: Principles, Measurements, and Applications*, 1994.
2   R. H. Ewoldt, M. T. Johnston and L. M. Caretta, in *Complex Fluids in Biological Systems: Experiment, Theory, and Computation*, ed. S. E. Spagnolie, Springer New York, New York, NY, 2015, pp. 207–241.
3   A. Z. Nelson, K. S. Schweizer, B. M. Rauzan, R. G. Nuzzo, J. Vermant and R. H. Ewoldt, *Curr. Opin. Solid State Mater. Sci.*, 2019, **23**, 100758.
4   Y. Wang, A. P. Kaur, N. Harsha Attanayake, Z. Yu, T. M. Suduwella, L. Cheng, S. A. Odom and R. H. Ewoldt, *Phys. Fluids*, , DOI:10.1063/5.0010168.
5   L. T. T. Nhung, I. Y. Kim and Y. S. Yoon, *Polym. 2020, Vol. 12, Page 2714*, 2020, **12**, 2714.